Korean J. Chem. Eng., 32(3), 436-445 (2015)
DOI: 10.1007/s11814-014-0264-3

pISSN: 0256-1115
eISSN: 1975-7220

Characterization of high-alumina coal fly ash based silicate material and its adsorption performance on volatile organic compound elimination

Guojun Yuan*,*, Jianbin Zhang*,**,†, Yongfeng Zhang*,**, Yinan Yan*, Xinxin Ju*, and Junmin Sun*,****

*College of Chemical Engineering, Inner Mongolia University of Technology, Huhhot 010051, China
**Insititute of Coal Conversion & Cyclic Economy, Inner Mongolia University of Technology, Huhhot 010051, China
***Wuhai Environmental Monitoring Center, Wuhai 016000, China
(*Received 7 May 2014 • accepted 3 September 2014*)

Abstract−A highly stable silicate material from high-alumina coal fly ash was prepared and characterized using X-ray diffraction, scanning electron microscopy (SEM), Fourier transform infrared (FTIR) spectroscopy, thermal analysis, X-ray photoelectron spectroscopy, and elemental analysis. The spectral results show that the silicate material was mainly composed of six elements, C, Ca, O, Si, Mg, and Al, in the form of Ca^{2+}, Mg^{2+}, Al^{3+}, SiO_3^{2-}, and CO_3^{2-} ions. Some adsorbed water and/or water of crystallization was also observed. The silicate material showed exceptionally high capability to adsorb volatile organic compounds (VOCs). The results of dynamic adsorption behavior show that the silicate material presents similar properties with commercial activated carbon and stronger absorption properties than commercial diatomite for the adsorption of VOCs. The FTIR spectral results show weak hydrogen bonding interactions of the silicate material with three VOCs.

Keywords: High-alumina Coal Fly Ash, Silicate Material, Volatile Organic Compounds, Column Breakthrough Curve, Hydrogen Bonding

INTRODUCTION

The emission of volatile organic compounds (VOCs) causes air pollution in both indoor and outdoor air [1]. VOCs are noxious and/or carcinogenic [2,3], creating many severe environmental problems including adverse effects on human health at very low concentrations [4,5]. Technologies are being developed to reduce VOC emission [6] to comply with the latest environmental regulations. Various alternatives are available such as thermal oxidation, catalytic oxidation [7], photocatalytic oxidation [8,9], biofiltration, adsorption, absorption, condensation, and membrane separation. Among them, adsorption technology [10,11] without chemical degradation is a preferred strategy, particularly when the captured organic pollutants have alternative uses [12]. The primary requirements for adsorbents used in industrial process include sufficient adsorptive capacity, high adsorption rate, and low cost [13,14].

With the aim of increasing the efficiency of VOC removal, adsorption mechanism of the interactions between materials and VOCs has been studied. Several adsorbents such as activated carbon [15], hydrophobic zeolite [16,17], and mesoporous silica [18,19] have attracted much interest to control VOC emission. Activated carbon [20] is widely used because of its high micropore volume and low operating cost. However, activated carbon has several disadvantages such as fire risk, pore blocking, hygroscopicity, and a lack of regenerative ability. Hydrophobic zeolites are effective in VOC removal; however, high diffusion restrictions forced by the micropores inhibit the adsorption of large VOC molecules. Ordered mesoporous silicas such as SBA-15 [21], MCM-41 [22,23], MCM-48 [24], Si-MCM-41 [25] and KIT-6 [26] have attracted considerable attention to control VOCs because of their high surface area, high porosity, controllability, narrowly distributed pore sizes and good mechanical stability. However, ordered mesoporous silicas are not widely adopted in the industry process due to their high operating cost. Therefore, the use of cheaper silica material would be a great contribution to industrial applications. Several research studies have attempted to recover the silica materials from the waste products [27-32].

Coal fly ash (CFA) generated during the combustion of coal in coal-fired power stations is an industrial by-product, and it is a recognized environmental pollutant if not put to beneficial use. The principal components of bituminous coal fly ash are silica, alumina, iron oxide, and calcium, with varying amounts of carbon [33]. High-alumina coal fly ash (HACFA) in parts of Inner Mongolia, China, contains 40-50% of alumina total mass in the ash, and an estimated 12 million tons of HACFA is produced in Inner Mongolia every year, with approximately 100 million tons of HACFA accumulated over the years [34]. Hence, recycling HACFA can be a good alternative to disposal with significant economic and environmental benefits [35]. Recently, much effort has been made to recycle CFA [36]. For example, ~20% CFA is used in concrete production. Other uses include soil amelioration [37,38], ceramic industry [39-41], catalyst and catalyst support [42-44], adsorbents for pollutant removal [45,46], depth separation [47], zeolite synthesis [48-50], valuable metal recovery [51,52] and alumina extraction from HACFA [34, 53]. However, the preparation of silicate materials from HACFA has not been reported.

†To whom correspondence should be addressed.
E-mail: tadzhang@pku.edu.cn
Copyright by The Korean Institute of Chemical Engineers.

The objective of this study was to investigate the surface characteristics and adsorption performance of HACFA-based silicate material for VOCs such as formaldehyde, toluene, and benzene. The dynamic and static adsorption behavior of VOCs on the surface of silicate material was investigated by continuous flow adsorption and weight measurements. Furthermore, the adsorption behaviors of the three VOCs on the silicate material were analyzed by scanning electron microscopy (SEM) and Fourier transform infrared (FTIR) spectroscopy.

EXPERIMENTAL

1. Adsorbent

HACFA, whose price is ~0.32 US dollars per 1 kg used in this study, was obtained from pulverized coal-fired boilers of thermal power plants located in Inner Mongolia, China. The alumina and silica content are 46.7% and 42.5%, respectively. The silicate material was synthesized from HACFA according to the published methods [54,55]. The detailed procedure had four major steps as shown in Fig. 1. First, 15% sodium hydroxide solution was prepared. Then the HACFA was added into sodium hydroxide solution, and the mass ratio of sodium hydroxide to HACFA was 0.5. The mixture was stirred at 120 °C for 120 min to complete the desilication process. When the desilication process completed, the mixture was subjected to filtration to get the sodium silicate extracts. After that, moderate lime milk was added into the sodium silicate extracts, and the mass ratio of calcium oxide to silica was about 0.5. The mixture was stirred at 90 °C for 60 min. Then, the mixture was subjected to filtration and washing with water, and the white precipitate was collected. The final calcium silicate particles product was obtained after drying at 350 °C for 60 min. The possible chemical reactions are as follows:

$$SiO_2+2OH^-=SiO_3^{2-}+H_2O$$
$$SiO_3^{2-}+Ca^{2+}=CaSiO_3\downarrow$$

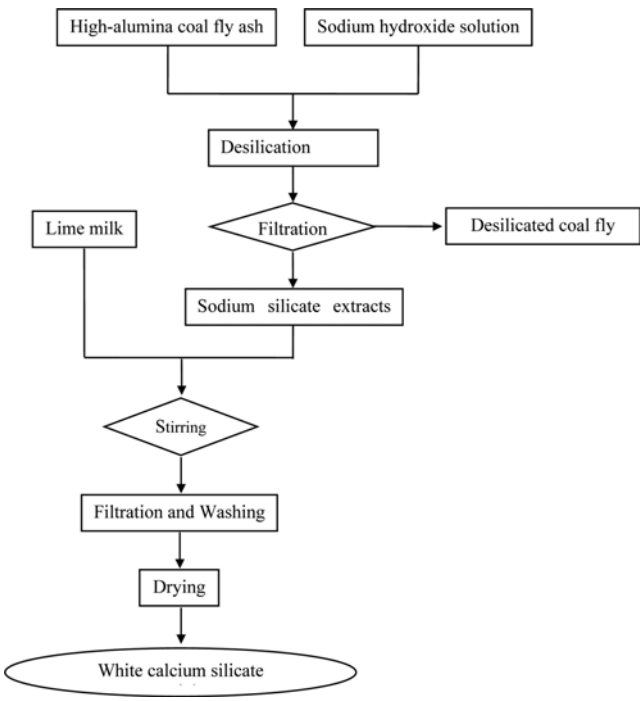

Fig. 1. Preparation process of silicate material.

Commercially available activated carbon (~4.19 US dollars per 1 kg), and diatomite (~2.42 US dollars per 1 kg) were used.

2. Adsorbent Characterizations

Powder X-ray diffraction (XRD) patterns were recorded within the 2θ range 20-80° with a constant 2θ step of 0.02° using a Bruker D8 Advance diffractometer with Cu Kα radiation and LynxEye detector. X-ray photoelectron spectroscopy (XPS) data were obtained with a KRATOS Axis ultra X-ray photoelectron spectrometer with a monochromatized Al$K\alpha$ X-ray (hν=1486.6 eV) operated at 150 W. Adsorption and desorption isotherms of nitrogen were measured with a 3H-2000PS2 gas sorption analyzer at liquid nitrogen temperature (−196 °C). Before the measurements, all the samples were degassed under vacuum at 150 °C for 4 h. The Brunauer-Emmett-Teller (BET) method was used to calculate the specific surface area using the adsorption data acquired at a relative pressure (P/P_0) range 0-1.0. The total pore volume was estimated from the amount adsorbed at a relative pressure of ~0.99. The FTIR spectra (KBr pellets) were recorded using a Nexus 670 FTIR spectrometer with a resolution of 1 cm^{-1} accumulating 32 scans, and a base line correction was made for the spectra, which were recorded in air. Thermal analysis that includes thermogravimetry (TG) and differential thermal analysis (DTA) of the original silicate material were performed using a TG/DTA analyzer (STA PT1600, Germany), and the heating rate was 10 °C/min. SEM images were recorded using a S3400N to study the microstructure, textural properties, particle morphologies, and energy spectrum. All the solid reagents were weighed using a Sartorius BS224S electric balance.

3. Column Breakthrough Curves

The adsorption experiments for low concentration VOCs, including formaldehyde, toluene, or benzene, were carried out using a continuous experimental apparatus. The setup consisted of a glass column equipped with a thermostatic jacket, an evaporation chamber, a volumetric gas meter, and a cold thermostat bath. All the experimental runs were performed with dry air supplied by a gas cylinder at a constant flow rate. The system used to measure the adsorption of the mixture consisted of a fixed bed reactor with an internal diameter of 6 mm coupled to a mass spectrometer. Pellets of the silicate material were packed in a fixed bed. The N_2/VOC mixture obtained using a bubbler was diluted with dry air and injected at the bottom of the column. The samples were collected at the inlet and outlet of the column. The temperature used for the adsorption experiments was 298 K. The bed contained ~0.2 g of the silicate material, and the flow rate of the gas during the experiments was 502 mL/min. The concentrations at outlet and inlet of the apparatus were similar, indicating that equilibrium was reached. In the experiments, the relative pressures of both the pollutants were different, because the gas concentrations were the same and the saturation pressures of each VOC were different.

4. Dynamic Adsorption Measurements

The adsorption experiments were in a fixed bed continuous flow reactor at various temperatures (see Fig. 2). Before the adsorption measurements, each sample was degassed overnight at 150 °C. The

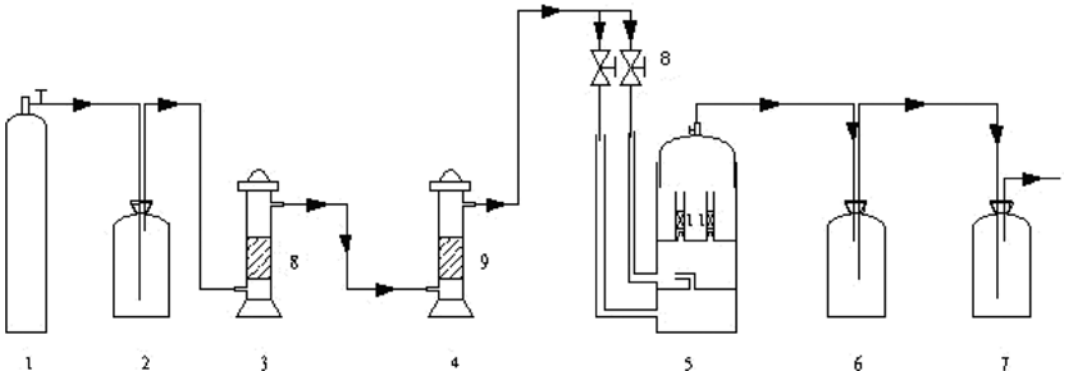

Fig. 2. Adsorption apparatus for dynamic test.
1. N_2 gas cylinder, 2, 6, 7. Buffer bottle, 3, 4. N_2 purifier, 5. Adsorption bottle, 8. Regulating valve

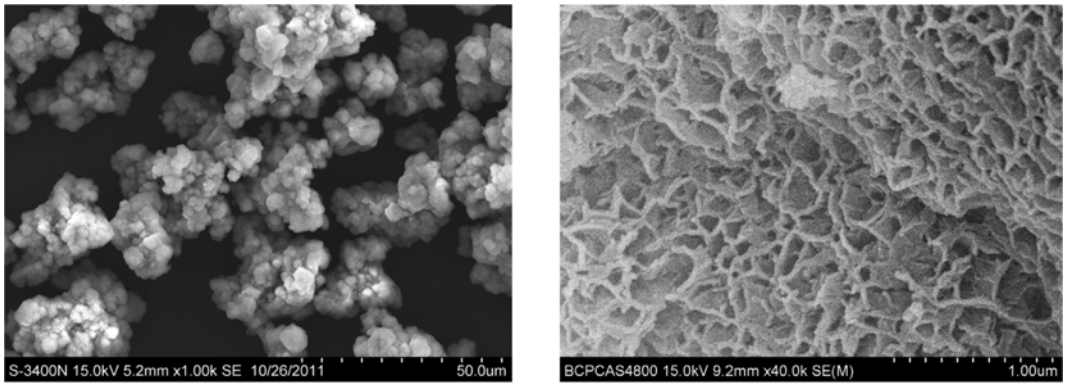

Fig. 3. SEM images of silicate material.

dynamic adsorption behavior was investigated to further study the effects of surface chemistry on the adsorption properties of the silicate material, and the adsorption properties of the silicate material for the three VOCs were compared with commercial activated carbon and diatomite at 298.15 K. The dynamic adsorption behavior was studied by keeping the three VOCs (formaldehyde, toluene, and benzene) in the adsorption apparatus. The amounts of VOCs adsorbed were calculated by the cutting and weighing method after the adsorption of VOCs on the adsorbent in the fixed bed. The speed of carrying gas was controlled at 30 mL/min. The temperature in the saturator was maintained using a constant temperature vessel.

RESULTS AND DISCUSSION

1. Characterizations of Silicate Material

1-1. SEM Analysis

Particle morphology is useful for understanding the physical properties of material, and the microstructure of material affects the binding and sorption properties. A distinct surface morphology of the silicate material was observed by the SEM images (Fig. 3).

The SEM images show that the silicate material is faveolate and consists of particles with irregular shape and size. A significant fraction of the particles have a rough surface, and others formed unevenly shaped aggregates. The particles of the silicate material have a diameter of 20-30 μm (Fig. 2(a)), and the silicate material has a lamina structure with a thickness of ~30 nm and faveolate structure with a diameter of 1-2 μm (Fig. 2(b)). The silicate material provided a rough surface for VOC adsorption, as suggested by the BET results.

The elements of the silicate material were analyzed using the en-

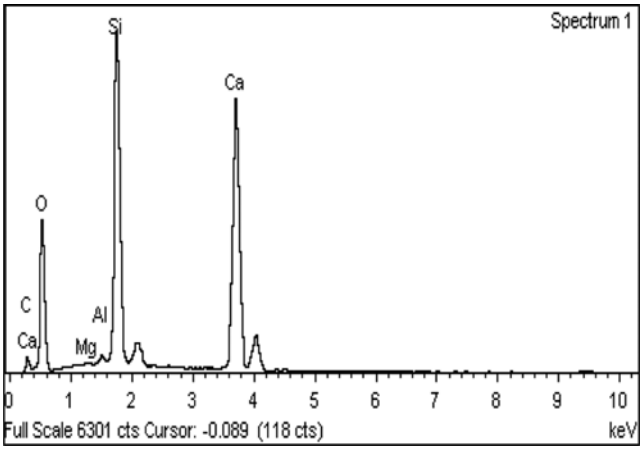

Fig. 4. Energy spectrum of silicate material.

Table 1. Element content for surface of silicate materials

Element	Weight%	Atomic%
C	6.24	10.38
O	51.81	64.76
Mg	0.22	0.18
Al	0.34	0.25
Si	17.69	12.60
Ca	23.70	11.82

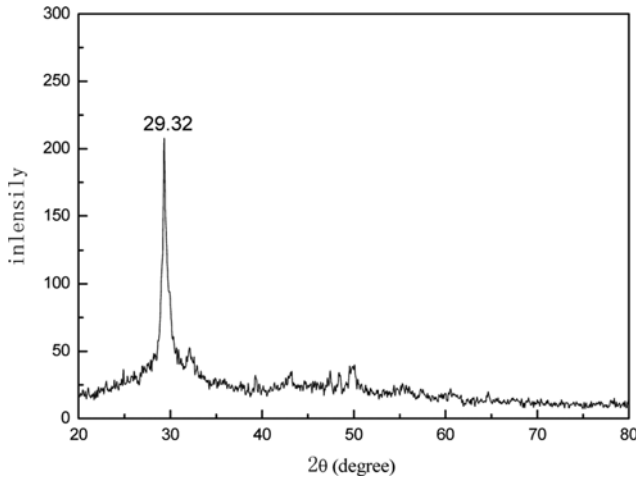

Fig. 5. XRD spectrum of silicate material.

ergy spectrum configured on the SEM. The energy spectral results of the material are shown in Fig. 4, and the element analysis results

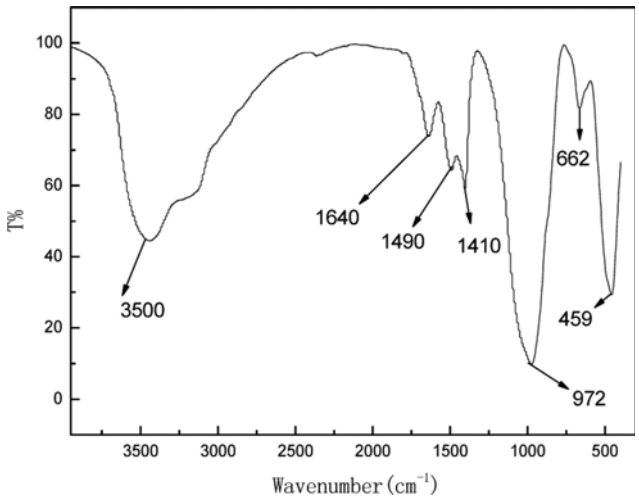

Fig. 6. FTIR spectrum for silicate material.

are listed in Table 1.

Table 1 shows that the silicate material is mainly composed of six elements, Ca, Si, Al, O, C, and Mg. The element content for surface of silicate materials is 64.76% O, the 10.38% C, and 12.60% Si. Based on the results from the energy spectrum and the following FTIR spectrum, SiO_3^{2-} and CO_3^{2-} may be present in the silicate material.

1-2. XRD Analysis

The XRD patterns of the original silicate material were recorded as shown in Fig. 5.

From Fig. 5, a diffraction peak at 29.32° was observed, which is

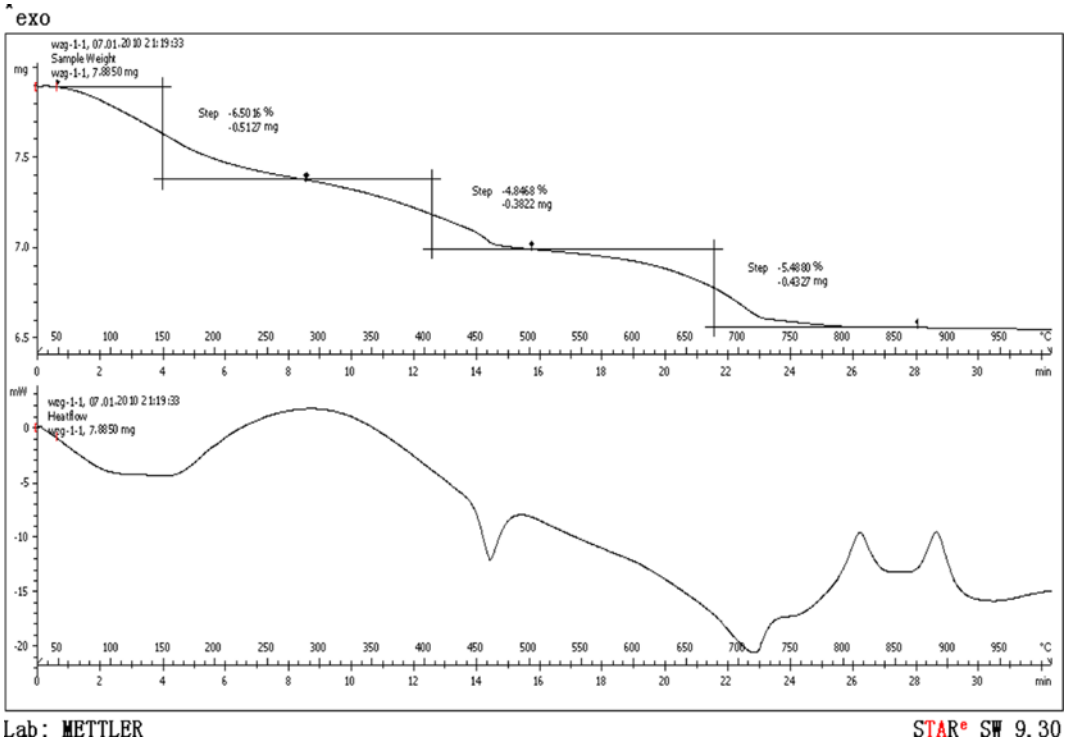

Fig. 7. TGA-DTA spectrum of silicate materials.

characteristic of calcite [56,57]. The results implied that the obtained silicate material was amorphous and some calcite presents in the silicate material. Moreover, the XRD results show that some impurities may exist in the silicate material.

1-3. FTIR Spectral Analysis

Fig. 6 shows the FTIR spectrum of the silicate material.

The FTIR spectrum shows a broad band at ~3,500 cm^{-1}, which can be attributed to the O-H groups in Si-O-H and H_2O, and a peak at 1,640 cm^{-1} [58,59], which can be attributed to the H-O-H bending vibration in H_2O. The spectrum shows the presence of adsorbed water and/or water of crystallization in the material. The peaks at ~1,490 cm^{-1} and 1,410 cm^{-1} can be attributed to the stretching vibration bands of CO_3^{2-}. The peak at 972 cm^{-1} can be attributed to the Si-O stretching vibration [1], and the peak at 459 cm^{-1} can be attributed to the Si-O bending vibration [59]. The FTIR spectral results clearly confirm that the silicate material contains Si-OH, SiO_3^{2-}, and CO_3^{2-}.

1-4. TGA-DTA Analysis

The thermal stability of the silicate material was observed by TGA-DTA analysis, as shown in Fig. 7.

The silicate material showed a total mass loss of 1.3276 mg (16.83%) between 296 and 1,173 K. The initial weight loss of 6.5% until 463 K can be attributed to the moisture content in the sample [60] (the loss of molecular water from the exchange layer "interlayer water"). The amount of water uptake by the silicate material sample depends on the relative humidity of the exposed environment.

The second weight loss occurs at 773 K due to the removal of water composition from the silicate mineral [61]. The third weight loss occurring in the sample corresponds to the dehydroxylation of the silicate material. This is shown as a peak centered at 1,143 K in the DTA curve. The weight loss during the dehydroxylation of the studied silicate material sample was ~5.49% between 773 and 1,143 K and corresponds to the decomposition of $CaCO_3$ [60].

1-5. Isotherms

Fig. 8 shows the nitrogen adsorption-desorption isotherms of the silicate material.

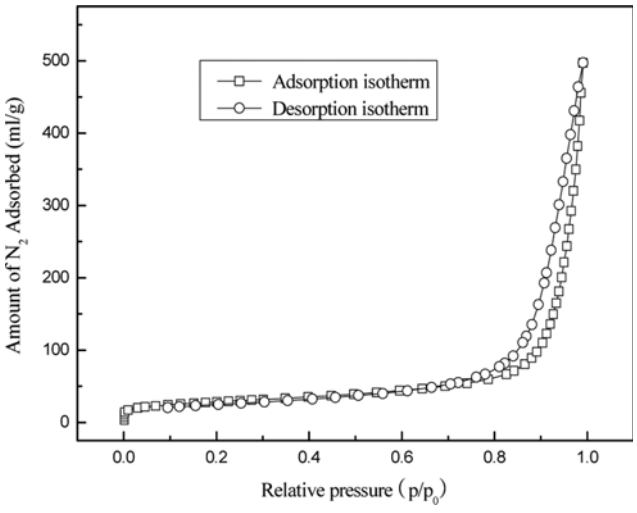

Fig. 8. Nitrogen adsorption-desorption isotherms of silicate material.

Table 2. Physical properties characterized by BET analysis

Material	S_{BET} [a] (m^2/g)	V_p [b] (ml/g)	d_{BJH} [c] (nm)
Silicate material	98.47	0.77	31.42

[a]BET specific surface area
[b]Pore volume
[c]Pore diameter calculated by BJH method

The sample exhibited type III isotherm based on the IUPAC classification.

The quantity of nitrogen adsorption sharply increased at a relative pressure (P/P_0) of 0.8, confirming the capillary condensation of nitrogen within the primary mesopores. The physical properties, such as the BET specific surface area, specific pore volume, and average pore diameter, of the silicate material are summarized in Table 2.

The silicate material has a specific surface area of 98.47 m^2/g. The pore size distribution of the silicate material was calculated from the nitrogen desorption isotherm using the Barrett-Joyner-Halenda (BJH) model. The results show a narrow distribution centered at 31.42 nm. The adsorption studies indicate the presence of poorly defined mesopores and thick, dense wall structure. On the other hand, the average pore diameter and specific pore volume of the silicate material indicate the possible adsorption sites for various gases.

1-6. XPS Analysis

Fig. 9 shows the XPS spectrum of the silicate material sample.

The spectrum shows two bands with peak positions at 287 and 283 eV for C 1s corresponding to a C^{4+} species, a band with a peak position at 41 eV for Mg 2p corresponding to a Mg^{2+} species, a band with a peak position at 100 eV for Si 2p corresponding to a Si^{4+} species, a band with a peak position at 529 eV for O 1s corresponding to an O^{2-} species, and two bands with peak positions at 345 and 348 eV for Ca 2p corresponding to a Ca^{2+} species.

The above results and analyses show that the silicate material is composed of C, Ca, O, Si, Mg, and Al in the form of Ca^{2+}, Mg^{2+}, Al^{3+}, SiO_3^{2-}, and CO_3^{2-} ions. Some adsorbed water and/or water of crystallization was observed in the silicate material.

2. VOCs Removal Analysis

2-1. Column Breakthrough Curves

The removal of typical VOCs such as formaldehyde, toluene, and benzene by the silicate material was investigated by studying the adsorption column breakthrough curves. The investigation was first carried out for a single component adsorbate with a low concentration under dry conditions to evaluate the performance of VOC removal (Fig. 10).

Under dry conditions, the silicate material exhibited a breakthrough time of 15 h for formaldehyde (Fig. 10(a)) at 298 K when the inlet concentration of formaldehyde was 0.93 mg/m^3, and the silicate material showed the adsorption capability of 0.57 mg/g formaldehyde.

The silicate material exhibited a breakthrough time of 200 h for toluene (Fig. 10(b)) at 298 K when the inlet concentration of toluene was 3.75 mg/m^3, and the silicate material showed the adsorption capability of 54.05 mg/g toluene.

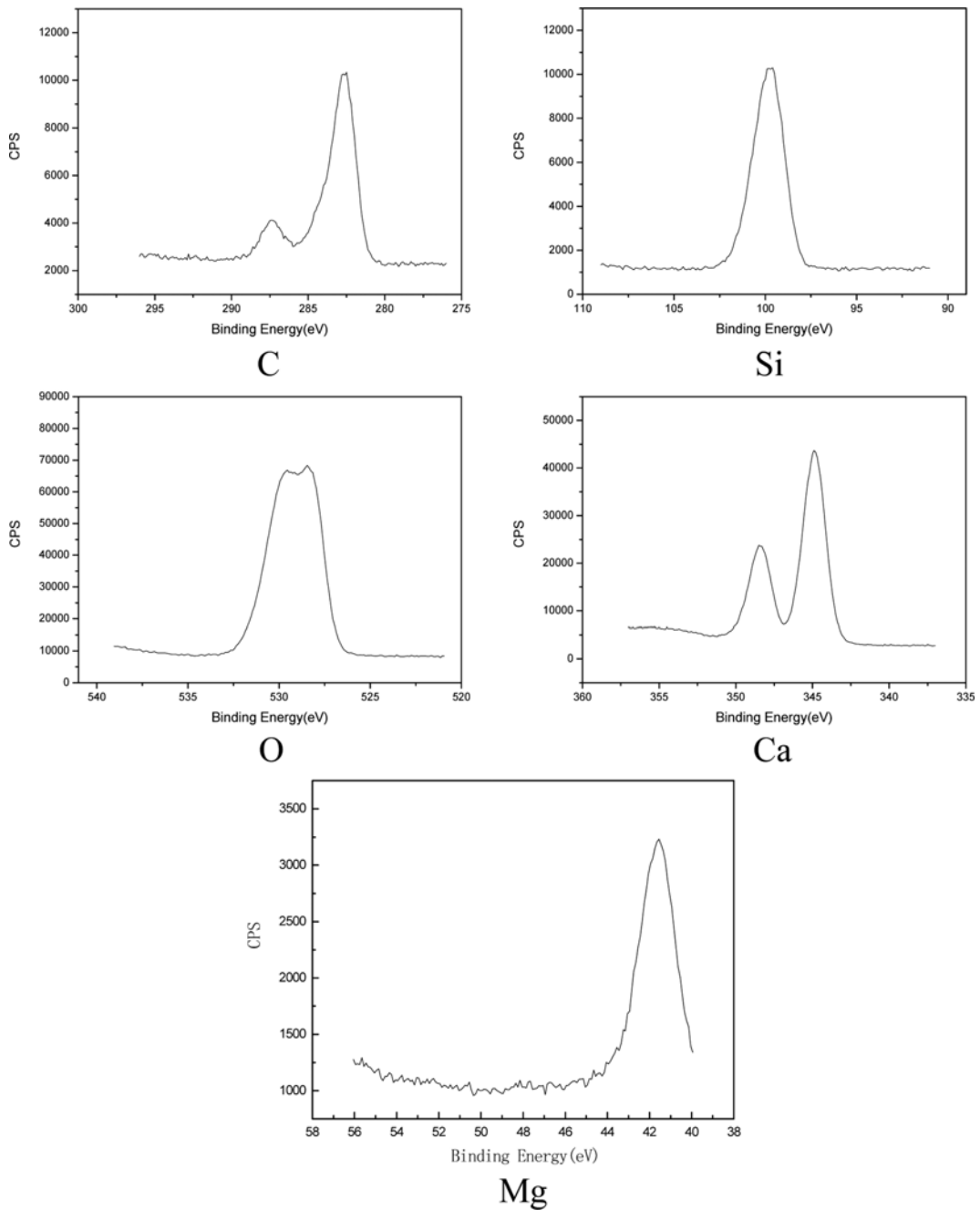

Fig. 9. XPS spectrum for the silicate material.

In addition, the silicate material exhibited a breakthrough time of 80 h for benzene (Fig. 10(c)) at 298 K when the inlet concentration of benzene was 4.85 mg/m^3, and the silicate material showed the adsorption capability of 13.42 mg/g benzene.

Thus, the silicate material exhibits a higher adsorption capacity for toluene and a lower adsorption capacity for formaldehyde.

2-2. Dynamic Adsorption Behavior

The dynamic adsorption behavior was investigated to further study the effects of surface chemistry on the adsorption properties of the silicate material, commercial diatomite, and commercial activated carbon at 298.15 K for high concentration. The dynamic adsorption behavior was studied by keeping the three adsorbed materials (formaldehyde, toluene, and benzene) in the adsorption apparatus (Fig. 2). N_2 gas was passed through the apparatus. After certain adsorption time, the silicate materials were weighed, and the adsorption data were recorded. The adsorption isotherms of the three VOCs on the three materials are shown in Fig. 11.

Fig. 11(a) shows that 1 g commercial activated carbon can adsorb 0.50 g formaldehyde when the dynamic adsorption equilibrium is reached. Under the same conditions, 1 g silicate material can adsorb 0.33 g formaldehyde, and 1 g commercial diatomite can adsorb 0.23 g formaldehyde.

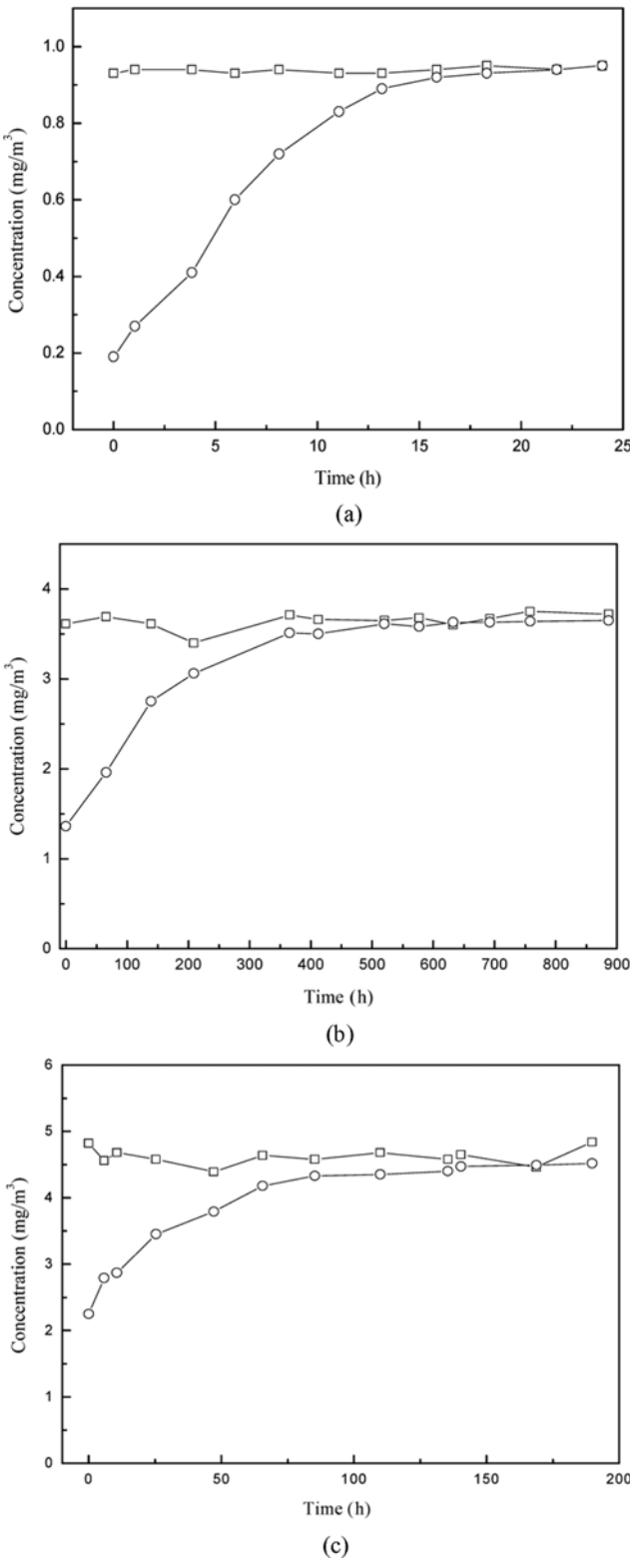

Fig. 10. Breakthrough curves of silicate material adsorbing formaldehyde (a), toluene (b), and benzene (c). □ Inlet concentration; ○ exit concentration.

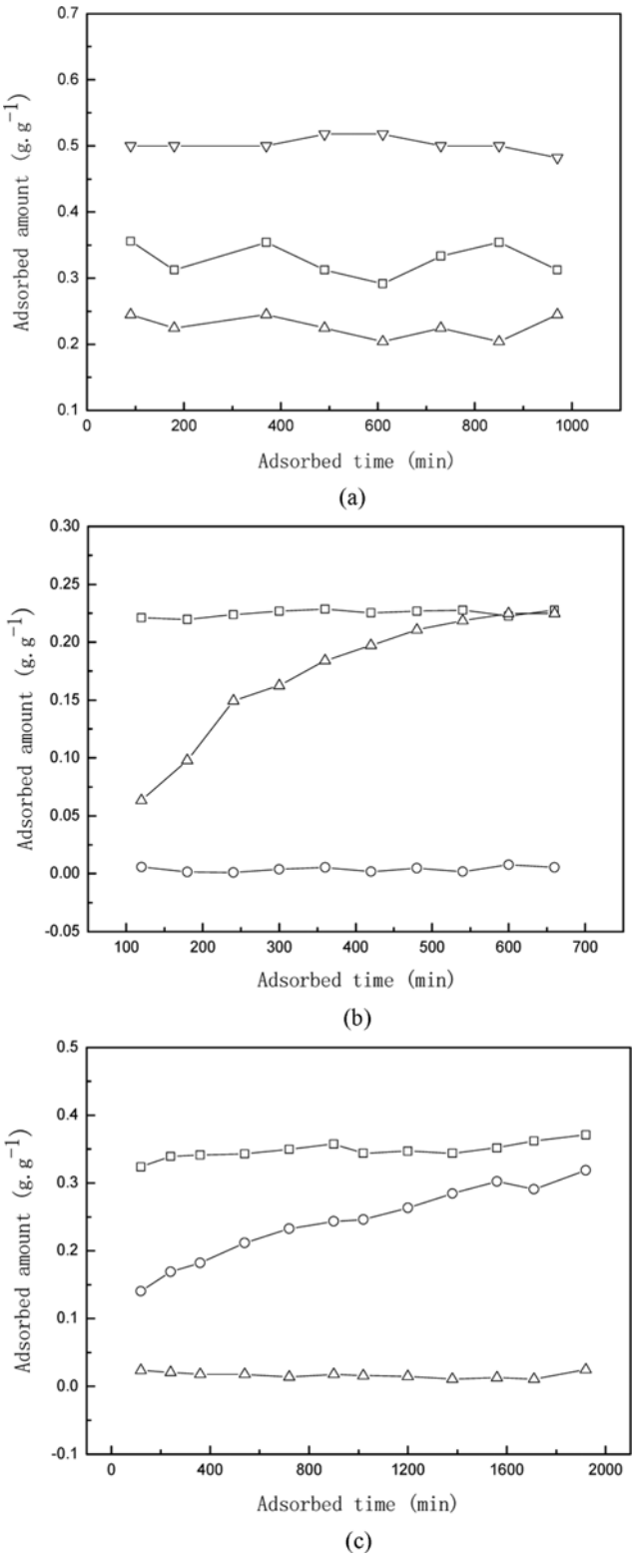

Fig. 11. Dynamic adsorption of different adsorbent for formaldehyde (a), benzene (b), and toluene (c). □ Silicate material; △ diatomite; ▽ active carbon.

Fig. 11(b) shows that 1 g commercial activated carbon can adsorb 0.35 g toluene when the dynamic adsorption equilibrium is reached. Under the same conditions, 1 g silicate material can adsorb 0.30 g toluene, and 1 g commercial diatomite can adsorb 0.03 g toluene.

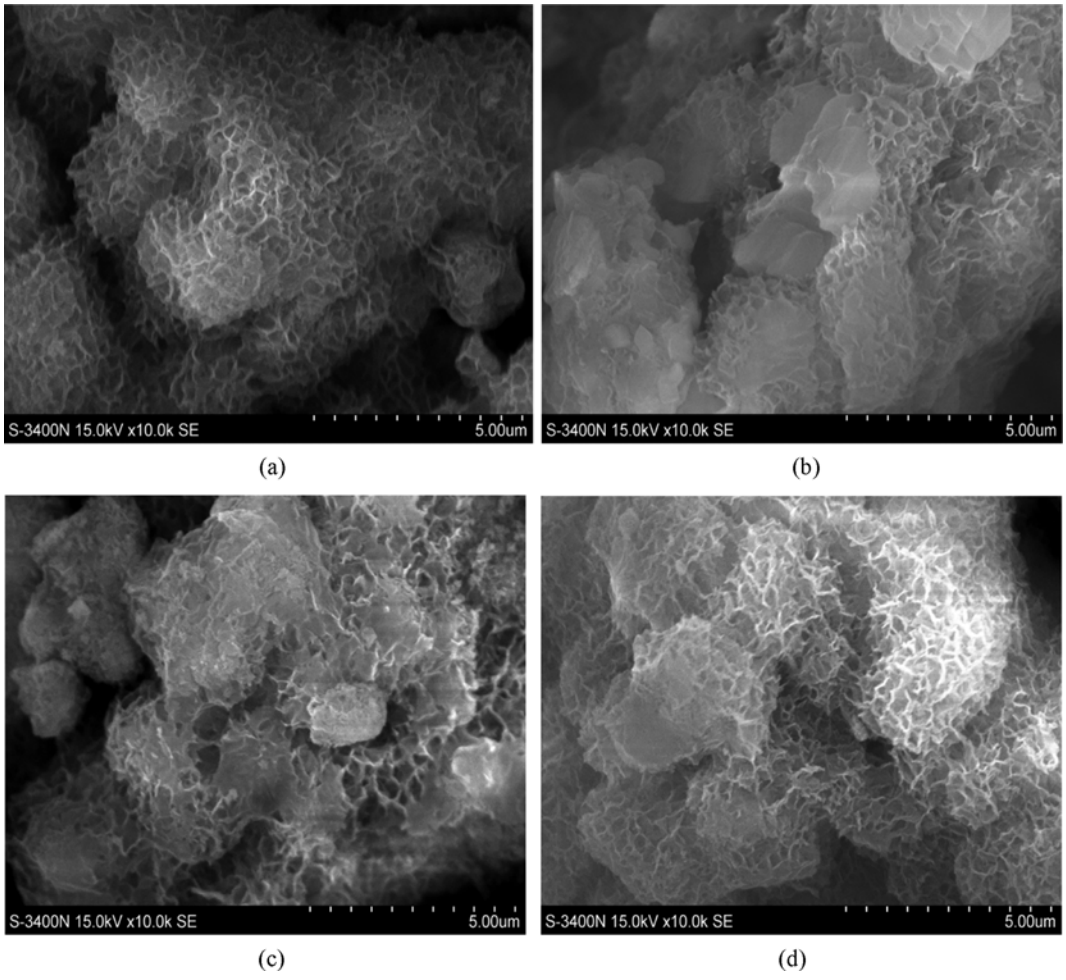

Fig. 12. SEM images of silicate materials before (a) and after adsorbing formaldehyde (b), toluene (c), and benzene (d).

Fig. 11(c) shows that 1 g commercial activated carbon can adsorb 0.23 g benzene when the dynamic adsorption equilibrium is reached. Under the same conditions, 1 g silicate material can adsorb 0.23 g benzene, and commercial diatomite almost does not adsorb benzene.

The dynamic adsorption experimental results show that commercial activated carbon has strong adsorption capability for the three VOCs. The silicate material exhibits similar adsorption capability as commercial activated carbon, and commercial diatomite exhibits low adsorption capability for the three VOCs.

2-3. SEM Images and FTIR Spectra

A variation in the surface morphology was observed by the SEM images (Fig. 12).

As shown by the SEM analyses, the silicate material has a faveolate structure and consists of particles with irregular shape and size. A significant fraction of the particles have a rough surface, and others formed unevenly shaped aggregates. The silicate material could adsorb the three VOCs by filling them in its micropores.

After the adsorption of the three VOCs on the silicate material, the FTIR spectrum was recorded as shown in Fig. 13.

The peaks at ~1,480 cm^{-1} can be attributed to the C=O stretching vibration after formaldehyde gas was adsorbed on the silicate material. The peak at 872 cm^{-1} can be attributed to the C=O bending vibration. The peak at ~1,460 cm^{-1} can be attributed to the asym-

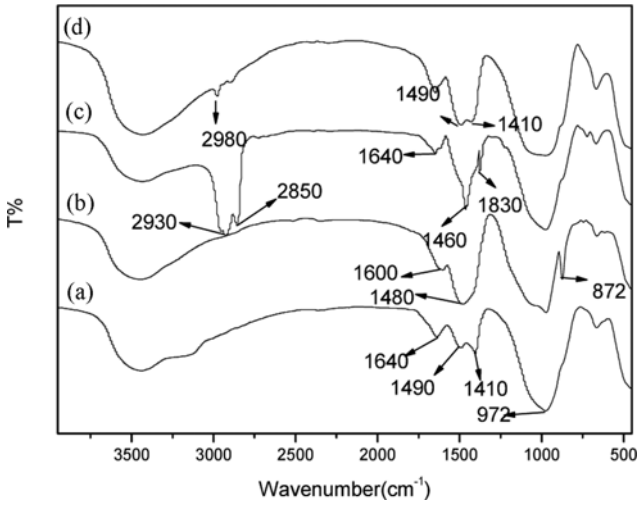

Fig. 13. FTIR spectra for the silicate material before (a) and after adsorbing formaldehyde (b), toluene (c), and benzene (d).

metric stretching vibration bands of CH_3 after toluene was adsorbed on the silicate material. The peak at 1,380 cm^{-1} can be attributed to the stretching vibration bands of CH_3. The peaks at 2,930 and 2,850 cm^{-1} can be attributed to the stretching vibration bands of CH in toluene. The peak at 717 cm^{-1} can be attributed to the stretching vibration bands of CH_3. The broad peaks at ~1,410 cm^{-1} and 1,490 cm^{-1} can be attributed to the C-H and C=C bonds in the benzene molecules after benzene was adsorbed on the silicate material. The peak at 2,980 cm^{-1} can be attributed to the stretching vibration band of CH in benzene.

In general, besides adsorbates, the adsorption capacity of the silicate material depends on the specific surface area, pore size distribution, and surface chemical properties [62]. Therefore, the estimation of relative contribution of VOC sorption mechanisms from the perspective of sorbate-sorbent molecular interactions would be practically useful. Small molecules (low van der Waals forces) are not easy to adsorb at low concentrations [63]. However, when formaldehyde molecules are adsorbed on the surface of the silicate material, the oxygen atom of the C=O bond in the formaldehyde molecules may interact with the hydroxyl hydrogen atom in the silicate material by hydrogen bonding, thus adsorbing the formaldehyde molecules on the silicate material. Formaldehyde acts as a hydrogen-bond donor (HBD) when it interacts with the Si-OH bond in the silicate material. Toluene and benzene exhibit similar sorption mechanisms. When toluene and benzene molecules were adsorbed on the silicate material, the adsorption processes were reversible processes occurring through van der Waals forces. The adsorbed toluene and benzene molecules can be easily generated for further adsorption cycles. This is because the adsorption mechanism proceeds through monolayer to multilayer adsorption as the VOC partial pressures of the gas phase in the adsorption system approaches the saturation pressure of the solvent at that temperature, and the smaller silicate material pores become filled with VOC molecules.

In short, the silicate material was synthesized from HACFA and characterized using XRD, SEM, FTIR spectroscopy, thermal analysis, XPS, and elemental analysis, and the pore size distributions were calculated from the nitrogen sorption studies. The spectral results and analyses show that the silicate material is composed of C, Ca, O, Si, Mg, and Al in the form of Ca^{2+}, Mg^{2+}, Al^{3+}, SiO_3^{2-}, and CO_3^{2-} ions. Some adsorbed water and/or water of crystallization was observed in the silicate material. The price of the silicate material is ~0.32 US dollars per 1 kg; therefore, the mesoporous material can also be applied as an adsorbent for three VOCs, including formaldehyde, toluene, and benzene, as catalyst supports, adsorbents, and separation materials.

CONCLUSION

Silicate material was synthesized from HACFA and characterized using XRD, SEM, FTIR spectroscopy, thermal analysis, XPS, and elemental analysis, and the pore size distributions were calculated from the nitrogen sorption studies. The spectral results and analyses show that the silicate material is composed of C, Ca, O, Si, Mg, and Al in the form of Ca^{2+}, Mg^{2+}, Al^{3+}, SiO_3^{2-}, and CO_3^{2-} ions. Some adsorbed water and/or water of crystallization was observed in the silicate material. Under dry conditions, the silicate material exhibited a breakthrough time of 15 h for formaldehyde at 298 K when the inlet concentration of formaldehyde was 0.93 mg/m^3, and the material showed the adsorption capability of 0.57 mg/g formaldehyde; the material exhibited a breakthrough time of 200 h for toluene when the inlet concentration of toluene was 3.75 mg/m^3, and the material showed the adsorption capability of 54.05 mg/g toluene. In addition, the material exhibited a breakthrough time of 80 h for benzene when the inlet concentration of benzene was 4.85 mg/m^3, and the material showed the adsorption capability of 13.42 mg/g benzene. And the silicate material exhibits a higher adsorption capacity for toluene and a lower adsorption capacity for formaldehyde.

ACKNOWLEDGEMENT

This work was supported by the Program for New Century Excellent Talents in University (NCET-12-1017), the Program for Grassland Excellent Talents of Inner Mongolia Autonomous Region, Program for Young Talents of Science and Technology in Universities of Inner Mongolia Autonomous Region, National Natural Science Foundation of China (21466028), the Research Fund for the Doctoral Program of Higher Education of China (20111514120002), the Inner Mongolia Talented People Development Fund, and Yongfeng Boyuan Industry Co., Ltd. (Jiangxi Province, China).

REFERENCES

1. T. Tsoncheva, G. Issa, T. Blasco, M. Dimitrov, M. Popova, S. Hernandez, D. Kovacheva, G. Atanasova and J. M. L. Nieto, *Appl. Catal. A-Gen.*, **453**, 1 (2013).
2. S. L. Herren-Freund, M. A. Pereira, M. D. Khoury and G. Olson, *Toxicol. Appl. Pharm.*, **90**, 183 (1987).
3. R. Crebelli and A. Carere, *Mutat. Res.: Rev. Mutat. Res.*, **221**, 11 (1989).
4. J. J. Shah and H. B. Singh, *Environ. Sci. Technol.*, **22**, 1381 (1988).
5. E. D. Dimotakis, M. P. Cal, J. Economy, S. M. Larson and M. J. Rood, *Environ. Sci. Technol.*, **29**, 1876 (1995).
6. F. K. Khan and A. K. Ghosal, *J. Loss. Prev. Proc.*, **13**, 527 (2000).
7. J. J. Spivey, *Ind. Eng. Chem. Res.*, **26**, 2165 (1987).
8. C. H. Ao and L. C. Lee, *Chem. Rev.*, **95**, 69 (1995).
9. M. R. Hoffiman, S. T. Martin, W. Choi and D. W. Bahnemann, *Chem. Rev.*, **95**, 69 (1995).
10. K. L. Foster, R. G. Fuerman, J. Economy, S. M. Larson and M. J. Rood, *Materials*, **4**, 1068 (1992).
11. R. Serna-Guerrero and A. Sayari, *Environ. Sci. Technol.*, **41**, 4761 (2007).
12. A. K. Ghoshal and S. D. Manjare, *J. Loss Prevent. Proc.*, **15**, 413 (2002).
13. D. P. Serrano, G. Calleja, J. A. Botas and F. J. Gutierrez, *Ind. Eng. Chem. Res.*, **43**, 7010 (2004).
14. M. Guillemot, J. Mijoin, S. Mignard and P. Magnoux, *Ind. Eng. Chem. Res.*, **46**, 4614 (2007).
15. M. A. Lillo-Rodenas, A. J. Fletcher, K. M. Thomas, D. Cazorla-Amoros and A. Linares-Soano, *Carbon*, **44**, 1455 (2006).
16. W. Rudziński, J. Narkiewicz-Michałek and P. Szabelski, *Langmuir*, **13**, 1095 (1997).

17. S. Brosillon, M. H. Manero and J. N. Foussard, *Environ. Sci. Technol.*, **35**, 3571 (2001).
18. K. Kosuge, S. Kubo, N. Kikukawa and M. Takemori, *Langmuir*, **23**, 3095 (2007).
19. S. Z. Qiao, S. K. Bhatia and D. Nicholson, *Langmuir*, **20**, 389 (2004).
20. C. Long, Y. Li, W. Yu and A. Li, *J. Hazard. Mater.*, **203-204**, 251 (2012).
21. Q. Hua, J. J. Li, Z. P. Hao, L. D. Li and S. Z. Qiao, *Chem. Eng. J.*, **149**, 281 (2009).
22. L. L. Bei, H. Tao and C. M. Ma, *J. Nanosci. Nanotechnol.*, **14**, 3163 (2014).
23. D. B. Patel, S. Singh and R. Bandyopadhyaya, *Micropor. Mesopor. Mater.*, **137**, 49 (2011).
24. Y. C. Su, H. M. Kao and J. L. Wang, *J. Chromatogr. A*, **1217**, 5643 (2010).
25. C. Hung, H. Bai and M. Karthik, *Sep. Purif. Technol.*, **64**, 265 (2009).
26. B. J. Dou, Q. Hu, J. J. Li, S. Z. Qiao and Z. P. Hao, *J. Hazard. Mater.*, **186**, 1615 (2011).
27. P. B. Sarawade, J. K. Kim, A. Hilonga and H. T. Kim, *J. Hazard. Mater.*, **173**, 576 (2010).
28. T. H. Liou, *J. Nanopart. Res.*, **14**, 869 (2012).
29. L. Y. Lin, J. T. Kuo and H. Bai, *J. Hazard. Mater.*, **192**, 255 (2011).
30. K. S. Hui and C. Y. H. Chao, *J. Hazard. Mater. B*, **137**, 1135 (2006).
31. M. Bhagiyalakshmi, L. J. Yun, R. Anuradha and H. T. Jang, *J. Hazard. Mater.*, **175**, 928 (2010).
32. H. L. Chang, C. M. Chun, I. A. Aksay and W. H. Shih, *Ind. Eng. Chem. Res.*, **38**, 973 (1999).
33. M. Ahmaruzzaman, *Prog. Energy Combust. Sci.*, **36**, 327 (2010).
34. H. Q. Li, J. B. Hui, C. Y. Wang, W. J. Bao and Z. H. Sun, **147-148**, 183 (2014).
35. Z. T. Yao, M. S. Xia, P. K. Sarker and T. Chen, *Fuel*, **120**, 74 (2014).
36. M. Ilic, C. Cheeseman, C. Sollars and J. Knight, *Fuel*, **82**, 331 (2003).
37. V. Manoharan, I. A. M. Yunusa, P. Loganathan, R. Lawrie, C. G. Skilbeck and M. D. Burchett, *Fuel*, **89**, 3498 (2010).
38. H. Lee, H. S. Ha, C. H. Lee, Y. B. Lee and P. J. Kim, *Bioresour. Technol.*, **97**, 1490 (2006).
39. M. Erol, S. Kucukbayrak and A. Ersoy-Mericboyu, *Fuel*, **87**, 1334 (2008).
40. M. Erol, S. Kucukbayrak and A. Ersoy-Mericboyu, *J. Hazard. Mater.*, **153**, 418 (2008).
41. J. Fang, G. Qin, W. Wei and X. Zhao, *Sep. Pur. Technol.*, **80**, 585 (2011).
42. D. Jain, C. Khatri and A. Rani, *Fuel Process. Technol.*, **91**, 1015 (2010).
43. E. Saputra, S. Muhammad, H. Q. Sun, H. M. Anga, M. O. Tadéa and S. B. Wang, *Catal. Today*, **190**, 68 (2012).
44. X. P. Xuan, C. T. Yue, S. Y. Li and Q. Yao, *Fuel*, **82**, 575 (2003).
45. S. B. Wang and H. W. Wu, *J. Hazard. Mater.*, **136**, 482 (2006).
46. Y. Li, F. Zhang and F. Xiu, *Sci. Tot. Environ.*, **407**, 5780 (2009).
47. M. Niewiadomski, J. Hupka, R. Bokotko and J. D. Miller, *Fuel*, **78**, 161 (1999).
48. M. Chareonpanich, T. Namto, P. Kongkachuichay and J. Limtrakul, *Fuel Process. Technol.*, **85**, 1623 (2004).
49. Z. T. Yao, Y. Ye and M. S. Xia, *Environ. Prog. Sustain.*, **32**, 790 (2013).
50. D. Wu, B. Zhang, L. Yan, H. Kong and X. Wang, *Int. J. Miner. Process.*, **80**, 266 (2006).
51. A. Hernandez-Exposito, J. M. Chimenos, A. I. Fernandez, O. Font, X. Querol, P. Coca and F. Garcia Pena, *Chem. Eng. J.*, **118**, 69 (2006).
52. F. Arroyo Torralvo and C. Fernández-Pereira, *Miner. Eng.*, **24**, 35 (2011).
53. A. Shemi, R. N. Mpana, S. Ndlovu, L. D. van Dyk, V. Sibanda and L. Seepe, *Miner. Eng.*, **34**, 30 (2012).
54. J. M. Sun, Z. J. Zhang, G. Chen, S. Y. Yan, Q. Z. Huo, L. C. Wu, H. L. Xu, L. A. Qin and X. X. Chen, CN. Patent, CN102249253A (2011).
55. Z. J. Zhang, J. M. Sun, H. F. Cao, X. Y. Zhang, Y. W. Wang and Q. Yao, CN. Patent, CN101591023 (2008).
56. R. R. Yadav, S. N. Mudliarb, A. Y. Shekh, A. B. Fulke, S. Saravana Devia, K. Krishnamurthi, A. Juwarkar and T. Chakrabarti, *Process Biochem.*, **47**, 585 (2012).
57. A. Sharma, A. Bhattacharya and A. Shrivastava, *Enzyme Microb. Technol.*, **48**, 416 (2011).
58. P. Tien and L. K. Chau, *Chem. Mater.*, **11**, 2141 (1999).
59. H. Zaitan, D. Bianchi, O. Achak and T. Chafik, *J. Hazard. Mater.*, **153**, 852 (2008).
60. M. V. Kok, *Energy Sources*, **24**, 899 (2002).
61. F. Ayari, E. Srasra and M. Trabelsi-Ayadi, *Desalination*, **185**, 391 (2005).
62. M. Guillemot, J. Mijoin, S. Mignard and P. Magnoux, *Appl. Catal. B-Environ.*, **75**, 249 (2007).
63. J. Tsai, H. Chiang, G. Huang snd H. Chiang, *J. Hazard. Mater.*, **154**, 1183 (2008).